Research Article

Talc-graphite schist as a natural organo-mineral complex for methylene blue remediation: kinetic and isotherm study

A. M. Zayed[1] · M. Fathy[2] · M. Sillanpää[3] · M. S. M. Abdel Wahed[1]

Received: 17 November 2019 / Accepted: 12 March 2020 / Published online: 21 March 2020

Abstract
Talc-graphite schist (TGSH) is a natural organo-mineral complex that was derived from the regional metamorphism of organic matter-bearing calcareous clays under the lowest temperature and pressure of the green schist facies (573–632 K and 1–3 Kbars, respectively). The application of TGSH that is widely available in the Meatiq area (Eastern Desert, Egypt) was investigated for the first time ever in the remediation of methylene blue dye (MB) from aqueous solutions. The characterization of the TGSH was carried out using various techniques (XRF, XRD, SEM, FT-IR and BET surface area), and its MB removal capacity was estimated at different experimental conditions. The MB adsorption by TGSH was time- and pH-dependent process, where 120 min was sufficient enough to attain equilibrium. The MB adsorption capacity by the TGSH was directly proportional to the applied temperature, confirming that the MB adsorption process was endothermic in behavior. Based on the determination coefficients, the pseudo-second-order equation ($R^2 = 0.939$) explained MB adsorption data better than the first-order one ($R^2 = 0.653$). Meanwhile, intra-particle diffusion was not the sole controlling rate in MB removal by the TGSH. Moreover, the nonlinear regressions of Langmuir model ($R^2 = 0.876$) explained the equilibrium data better than the other applied models (Temkin, $R^2 = 0.793$, and Freundlich, $R^2 = 0.752$). On the other hand, the estimated q_{max} (maximum removal capacity) of Langmuir was 9.41 mg/g at ambient temperature. Hydrogen bonding and electrostatic interaction were the governing mechanisms of MB removal by TGSH with variable impact in accordance with the prevailing pH condition.

Keywords Talc-graphite schist · Methylene blue removal · Adsorption kinetics · Adsorption isotherm · Nonlinear regressions

1 Introduction

Currently, the contamination of the aquatic systems with deleterious dyes from different industrial activities contributed in acute global environmental problem. The majority of these dye contaminants is not only nonbiodegradable but also has carcinogenic and/or mutagenic effect on health [57].

Methylene blue (MB) is approximately the most heavily applied cationic dyes for cotton, silk and wool dyeing [26, 24]. The discharge of MB-contaminated wastewater—even with low concentration (< 1 mg/L)—has a malignant impact not only upon the biological system of the aquatic environment, but also on the human being health in direct or in indirect way [64]. Consequently, MB remediation from industrial wastewater prior discharging is obligatory.

Various techniques have been utilized for MB remediation such as ozonation [83], coagulation [27], biological treatment [41], photocatalysis [34, 38] and membrane separation [13]. Although the success of these approaches,

✉ A. M. Zayed, ahmed.zayed@science.bsu.edu.eg; Zayed_2000eg@yahoo.com | [1]Applied Mineralogy and Water Research Lab, Geology Department, Faculty of Science, Beni-Suef University, Beni Suef, Egypt. [2]Egyptian Petroleum Research Institute, Cairo, Egypt. [3]Department of Green Chemistry, Faculty of Engineering Science, Lappeenranta University of Technology, Lappeenranta, Finland.

adsorption technique is still the favorable one for MB removal owing to economical and technical reasons [57]. Therefore, the utilization of natural materials such as clays [33], diatomites [52], perlite [22], zeolite [56], coal [31] and basaltic lava [48], has attracted the attention of researchers as effective, eco-friendly and cost-wise adsorbents.

Talc-graphite schist (TGSH) is low- to medium-grade metamorphic rock of greyish- to greyish-green color of green schist facies [30]. It was derived from intercalated passamo-pelitic sediments with biogenic materials in the form of organo-mineral complex (calcareous clays enriched with organic matters) via successive long-term metamorphic processes [9]. It belongs to Abu Fannani thrust sheet (ophiolitic mélange matrix) rock units that exposed at Meatiq domal area, Central Eastern Desert of Egypt [30]. Hundreds of millions of tons of the raw TGSH are available in Meatiq area and other different localities in the Eastern Desert (ED) of Egypt that are not adequately employed in any industrial activity till now and still waiting for the proper use. Therefore, the average price of TGSH is very low and never exceeds 100 EGP/ton in comparison with clays that exceed 600 EGP.

For the best of our knowledge, the application of the raw TGSH as a promising, widely available and low-cost alternative in MB removal was not evaluated before. Consequently, the main aims of the current work were (a) to investigate the ability of the Egyptian TGSH of Meatiq area in MB adsorption from aqueous solution (b) to weight the impact of the selected experimental parameters on MB adsorption efficiency by TGSH (c) to define the controlling mechanism of MB adsorption by TGSH and (d) to evaluate the influence of the adsorbed MB molecules upon the chemical, structural and morphological features of the spent TGSH.

2 Materials and Methods

2.1 Materials

Talc-graphite schist (TGSH) gathered from the Meatiq domal area in the ED of Egypt, methylene blue dye (MB) delivered from Fluka, Switzerland, and used without further processing, 97% purity NaOH (0.01 M) and HCl (0.01 M) (Alfa Aesar) for initial pH adjustment and ultrapure distilled water (DW), are the raw materials that were used in the current study.

2.2 Preparation of the raw talc-graphite schist

In total, 500 g of the grounded and sieved talc-graphite schist sample to less than 100 µm was quartered several times before soaking in distilled water with continuous stirring for 4 h. The decanted solid was dried over night at 343 K. After re-grounding and sieving to less than 100 µm size fraction, the produced powder was packed for application in MB removal from aqueous solution.

2.3 Talc-graphite schist characterization

X-ray fluorescence technique (XRF analyzer/PW/2404/Philips) was used to estimate the composition of the raw TGSH, while XRD diffraction pattern of the raw and spent TGSH was determined by a diffractometer (APD-3720/Philips) with a scanning speed 5°/min, Cu Kα radiation at 20 mA and 40 kV in the range from 5° to 80° of 2θ. The morphological characters of the pristine and the spent TGSH were defined by SEM (JSM-6700F/JEOL/Tokyo/Japan), while their functional groups were configured by FT-IR spectroscopy (Bruker FTIR-2000). Elemental analysis of the spent TGSH after MB removal was estimated by energy-dispersive X-Ray spectroscopy (EDS) equipped with SEM microscope.

After sample degassing in vacuum (373 K/180 min) to eliminate pore impurities, the pore diameter (D_p), pore volume (V_t) and the BET surface area (S_{BET}) of TGSH were estimated by "Quantachrome Surface Area Analyzer (Nova 2000)". The calculations of V_t and D_p were measured by the "Barrett–Joyner–Halenda (BJH)" equation [8], while S_{BET} was determined using "Brunauer–Emmett and Teller" equation [11].

Total organic carbon (TOC) and total carbon (TC) were determined for dried TGSH sample (at 378 K) using calibrated LECO SC-623 carbon analyzer device. TOC was estimated by treating an aliquot of the TGSH sample with 10% hot HCl to remove the inorganic carbon content prior to drying (at 378 K), as well as, the instrumental analysis. The total inorganic carbon (TIC)% in the studied TGSH was the result of the TOC subtraction from TC estimated percent.

2.4 Adsorption experiments

To prepare a MB stock solution (1.0 g/L), 1 g of MB was dissolved in 1000 mL of DW. This solution was diluted to the preferred initial concentration by DW for conducting equilibrium and kinetic studies.

For equilibrium tests, MB solution (25 mL) with various initial concentrations (40–140 mg/L) was separately mixed with a fixed mass of TGSH (0.3 g) and intensively agitated (200 rpm) for 120 min.

After liquid phase separation by centrifuging, the MB residual in solutions was estimated by a "Shimadzu UV–visible double beam spectrophotometer (Model UV 1601/Japan)" at $\lambda_{max} = 665$ nm. At equilibrium, the adsorbed amount of MB (q_e, mg/g) was estimated by Eq. (1) (Table 1).

For kinetic studies, the MB solution (25 mL/100 mg/L) was separately admixed with a fixed mass of the TGSH (0.3 g) for different retention time (5–240 min) with vigorous shaking at 200 rpm. Equations 2 and 3 (Table 1) were applied to calculate the removal capacity of MB (*R*%) and the adsorbed MB at equilibrium time *t* (q_t, mg/g) by the TGSH, respectively.

All experiments were performed in triplicate at room temperature (298 ± 2 K) with averaging the results.

2.5 Effect of the applied parameters (pH, concentration, adsorbent dose, agitation time and temperature)

To estimate the influence of the applied parameters on the removal behavior of MB by the pristine TGSH, batch mode was selected to perform all the experiments and the predominant experimental conditions for each of the investigated parameters are given in Table 2. At equilibrium, the separated liquids were used to measure the residual MB in the solutions.

3 Results and discussion

3.1 Characterization of talc-graphite schist

Chemically the pristine TGSH exhibited high SiO_2, MgO and CaO contents with a moderate amount of Fe_2O_3 (Table 3). The high loss on ignition value (LOI = 16.35%) reflected the hydrous nature of the TGSH mineral constituents, as well as its organic carbon content.

The XRD pattern of the TGSH revealed that talc-2M, actinolite, graphite and calcite are the dominant crystalline

Table 1 Equations of equilibrium and kinetic experiments of MB adsorption by raw TGSH

Equation no.	Linear form	Parameters
Equation 1	$q_e = \frac{V(C_i - C_f)}{m}$	q_e (mg/g): adsorbed amount of MB at equilibrium C_i: the initial MB concentration in solution (mg/L) C_f: the concentration of the adsorbed MB at equilibrium (mg/L) *V*: the volume of MB solution (ml) *m*: the mass of TGSH (mg)
Equation 2	$q_t = \frac{V(C_i - C_t)}{m}$	q_t (mg/g): adsorbed amount of MB at time *t* C_i: the initial MB concentration in solution (mg/L) C_t: the concentration of MB (mg/L) at time *t* *V*: the volume of MB solution (ml) *m*: the mass of TGSH (mg)
Equation 3	$R\% = \frac{(C_i - C_t)}{C_i} \times 100$	*R*%: removal efficiency of MB by TGSH C_i: the initial MB concentration in solution (mg/L) C_t: the concentration of MB (mg/L) at time *t*

Table 2 The applied experimental parameters and the prevailing condition during the conduction of their experiments

Investigated parameter	Conditions						The other parameters
pH	3	5	7	8	9	10	100 mg/L of MB initial conc., 0.3 g dose, 200 rpm/2 h (agitation time/speed), 25 ml solution volume, 298 K
Dose (g)	0.15	0.2	0.25	0.3	0.35	0.4	pH (9.0), 100 mg/L of MB initial con., 200 rpm/2 h (agitation time/speed), 25 ml solution volume, 298 K
Agitation time (min.)	5	15	30	60	120	240	pH (9.0), 100 mg/L of MB initial con., 0.3 g dose, 200 rpm agitation speed, 25 ml solution volume, 298 K
MB initial conc., (mg/L)	40	60	80	100	120	140	pH (9.0), 0.3 mg dose, 200 rpm/2 h (agitation time/speed), 25 ml solution volume, 298 K
Temperature (K)	298	308	318	323	328		pH (9.0), 100 mg/L of MB initial con., 0.3 g dose, 200 rpm/2 h (agitation time/speed), 25 ml solution volume

Table 3 Chemical composition of TGSH by XRF technique

Major component (%)/sample	SiO_2	TiO_2	Al_2O_3	Fe_2O_3	MnO	MgO	CaO	Na_2O	K_2O	P_2O_5	SO_3	Cl	LOI
TGSH	39.53	0.06	0.27	4.09	0.11	27.28	11.81	< 0.01	0.01	< 0.01	< 0.01	< 0.01	16.35

metamorphic phases, in association with a minor crystalline phase of quartz (Fig. 1a). The presence of these phases explains the high content of the above-mentioned major oxides in the TGSH. The minor presence of the amorphous noise in the XRD pattern of the TGSH confirms its high degree of crystallinity and its low organic carbon content (1.57%). The peaks of graphite reflect the presence of two structural varieties: hexagonal and trigonal graphite. The peak at 26.3° is related to the [002] reflection plane of the hexagonal structure [12, 35]; meanwhile, the minor peak at $2\theta = 43.5°$ is ascribed to [100] reflection plane of the rhombohedral phase of the graphite [60].

The main functional groups of the TGSH emerged at the following frequencies of the FT-IR spectra: 3740, 3664, 3419, 2925, 2860, 2516, 2384, 2307, 1798, 1425, 1017, 878, 760, 671 and 459 cm^{-1} (Fig. 1b). The stretching mode of the structural hydroxyl groups was correlated with the moderate intensity bands at 3740 and 3664 cm^{-1} [58, 15], while the band at 3419 cm^{-1} was assigned to both nitrogen-bearing (NH_2) group of the accompanying organic matters [45, 70] and to the stretching mode of water molecules [82]. Also the presence of the 2860 and 2925 cm^{-1} feeble bands is correlated with symmetric and asymmetric stretching vibration of C–H groups, correspondingly [16, 69, 42]. These C–H groups were also ascribed to the organic content of the TGSH. The very feeble bands at 2516, 2384 and 2307 cm^{-1} reflected the presence of CO_2 traces that were trapped in the structure of the TGSH [47], whereas the very weak band at 1798 cm^{-1} might confirm the existence of carbonyl group [49]. Furthermore, the existence of carbonate in the TGSH was confirmed by the stretching (strong band) and bending (shoulder band) modes of the CO_3^{2-} group at 1425 and 878 cm^{-1}, respectively [62]. Some studies also correlated the presence of the 1425 and 878 cm^{-1} bands to the C–O–H in the carboxylic group in a stretching mode [59] and to the Al–Fe–OH group as an indication for Mg enrichment [82].

Additionally, the bending and stretching modes of the siloxane group (Si–O–Si) were correlated with the very intense bands at 459 cm^{-1} [71] and 1017 cm^{-1} [18], respectively. Also the occurrence of quartz in the TGSH was reflected by the Si–O–Mg in stretching mode at 760 and 671 cm^{-1} [68].

SEM images indicated the flaky nature of the hydrous minerals of the pristine TGSH with occasional presence of regularly dispersed prismatic graphite crystals upon these flaky minerals (Fig. 2 a, b).

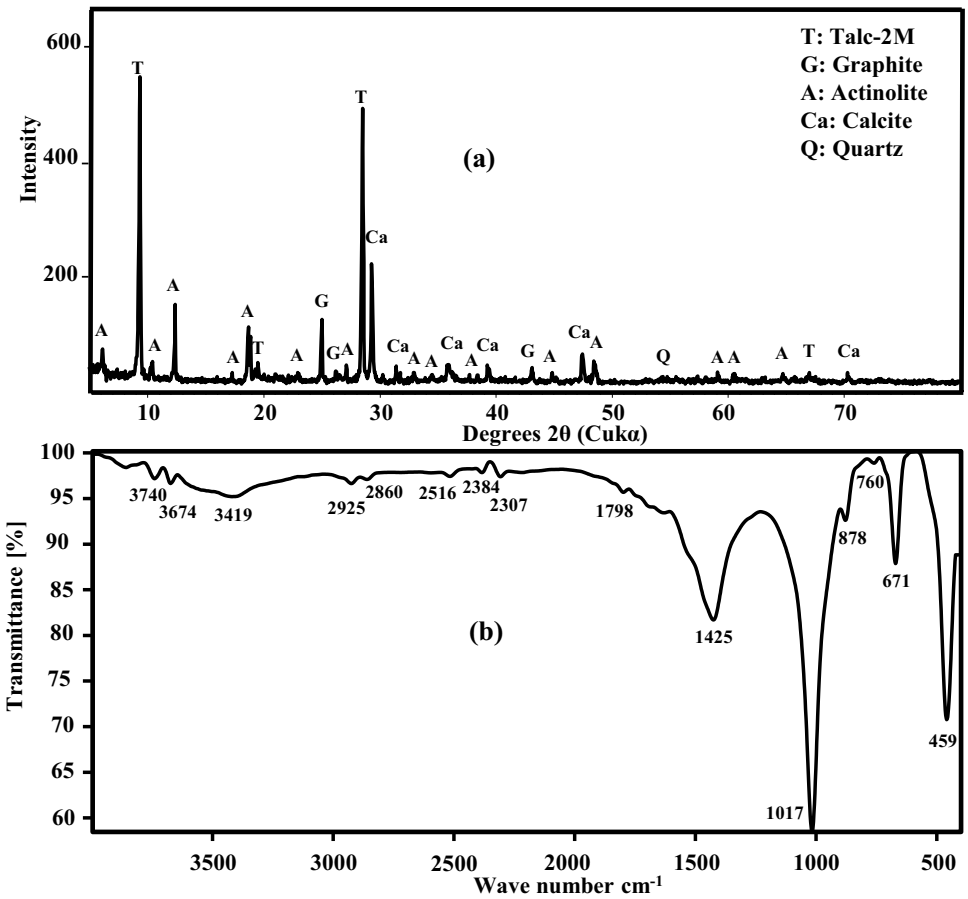

Fig. 1 XRD pattern of TGSH (**a**), FT-IR spectra of TGSH (**b**)

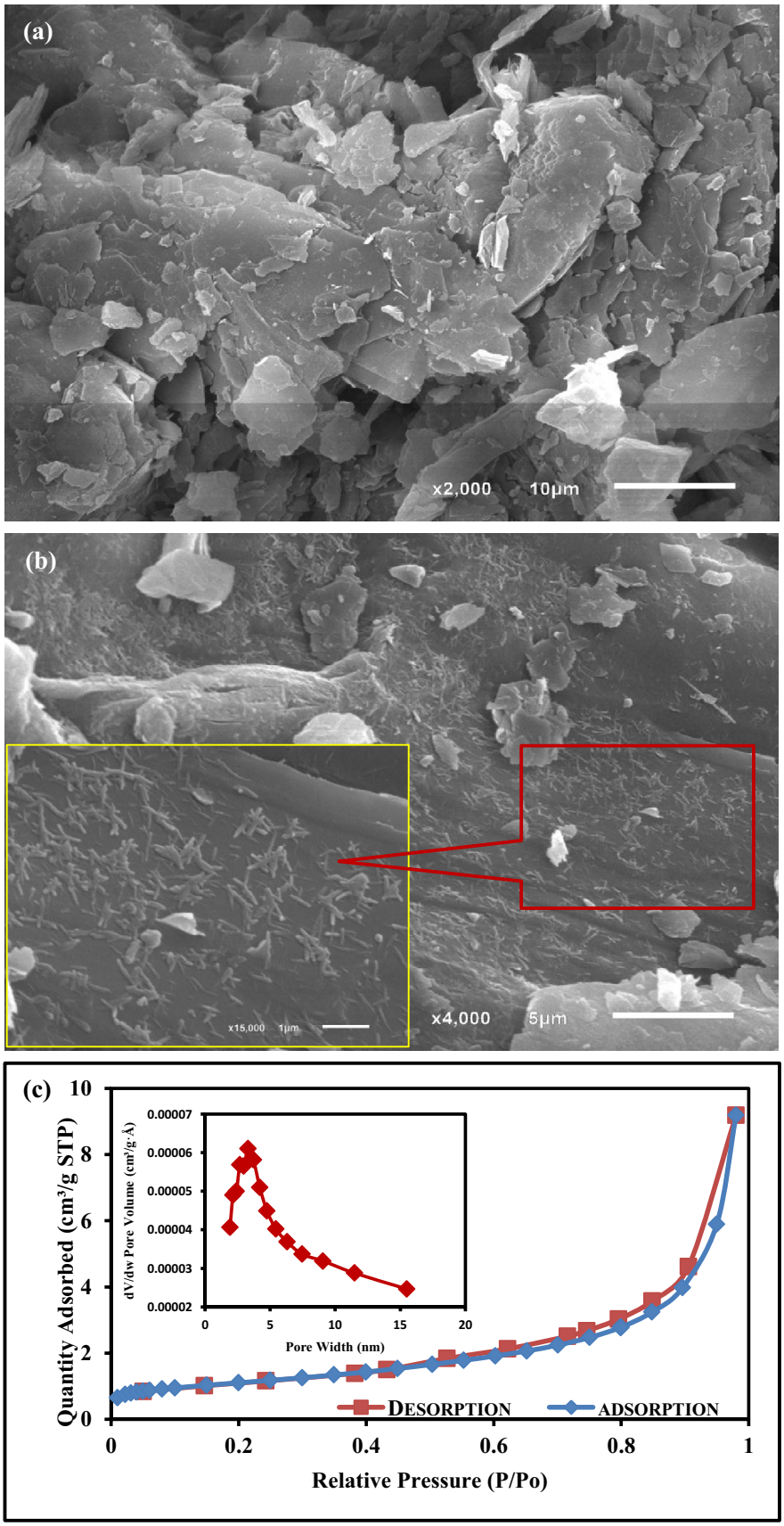

Fig. 2 SEM images with different magnifications for the pristine TGSH with hydrous minerals showing flaky nature and regularly dispersed prismatic graphite crystals on their surfaces (**a**, **b**), nitrogen adsorption–desorption isotherms for TGSH (**c**), BJH pore size distribution is shown in the inset

The TC, TOC and TIC analyses of the raw TGSH revealed that TIC content (3.27%) is noticeably exceeding the TOC content (1.57%). Moreover, TC content is about 4.84%. These results support the finding that the maturation of the carbonaceous impurities in the TGSH precursor (calcareous clays enriched in organic matters) into graphite was accomplished during the metamorphic processes (573–632 K, 1–3 kbars) to which the parent rocks were subjected.

The N_2 adsorption/desorption isotherm data revealed that the investigated TGSH displayed type II isotherm of the IUPAC classification with H_3 hysteresis loop (Fig. 2c). Such isotherm indicates the nonporous or macroporous nature of the studied TGSH [73]. This isotherm also indicated that mono-layer/multi-layer adsorption for nitrogen molecules occurred; the point of inflection from mono-($0 < P/P_o < 0.6$) to multi-layer ($P/P_o > 0.6$) adsorption appeared at P/P_o about 0.6 [63]. Also the overlapping of the two isotherm branches (adsorption/desorption) at $P/P_o < 0.6$ reflects the poor connectivity between the semi-closed pores of the TGSH, while the separation between those branches at relatively higher pressure ($P/P_o > 0.6$) indicates the presence of opened large pores in association with the semi-closed ones [50]. Moreover, the very poor geometrical parameters (Table 4) of the studied TGSH ($S_{BET} = 5.41$ m^2/g, $V_t = 0.0071$ cm^3/g) could be attributed to the close packing of the TGSH platy minerals during the experienced metamorphic processes that caused the emergence of these closed and semi-closed pores. Also as shown in the BJH curve (inset in Fig. 2c), the average pore diameter of the TGSH was 3.31 nm (Table 2).

3.2 Effect of solution pH

The applied initial pH played a conspicuous part in the MB removal from aqueous solution (Fig. 3a). By raising the initial pH from 3.0 to 8.0, the MB removal capacity (R%) increased from 83.8 to 89.9% before attaining equilibrium at pH 9.0 (R% = 93.2). Beyond pH 9.0, MB adsorption by TGSH displayed no appreciable increase in the R% (93.4%). These results are compatible with the zero charge point (pH_{PZC}) of the TGSH ($pH_{PZC} = 7.4$) that was determined according to Singh et al. [67] methodology (inset in Fig. 3a). The estimation of such pH can throw light upon the played role of the electrostatic attraction force in the removal of solute (MB) out of the aqueous system by the applied adsorbent [35], where, at $pH < pH_{PZC}$, the TGSH surface became protonated gradually with increasing medium acidity (i.e., positively charged surface) contributing in a progressive repulsive interaction between the positive MB ions and the nitrogen- and oxygen-bearing binding sites of the TGSH (amino, hydroxyl, carboxyl and siloxane groups), whereas, at $pH > pH_{PZC}$, the surface of the TGSH became negatively charged (i.e., de-protonated surface) motivating the attraction of the MB^+-hydrolyzed species toward the negatively charged active sites of the TGSH via electrostatic mechanism [2, 32, 65].

Although the overall improvement of MB removal capacity under basic conditions ($pH > pH_{PZC}$), electrostatic interaction (the nonhydrophobic adsorption driving forces) cannot be regarded as the only mechanism for MB adsorption by TGSH and contributions from other mechanisms (hydrogen bonding) acted as a driving force for MB adsorption, especially at $pH < pH_{PZC}$ [74]. Such potential mechanism can be ascribed to the hydrophobic nature of TGSH that was gained from the presence of talc, graphite and organic matter constituents of TGSH [5, 79]. The involvement of hydrogen bonding mechanism was assured by the high MB removal capacity at pH 3.0–5.0 (> 82%) although the strong competition from the available H^+ ions in the solution. Two sorts of hydrogen bonding interaction were involved in the MB removal process by TGSH: (a) dipole–dipole H-bonding, (b) Yoshida H-bonding. These interactions occurred between the available hydrogen atoms of the functional groups on the surface of TGSH and nitrogen atoms, as well as, the aromatic rings of MB dye, orderly [35, 74].

The adequate adsorption behavior of TGSH for MB ions in both acidic (> 80%) and basic (> 90%) mediums was attributed to its complex nature and hence the involvement of various functional groups in the adsorption process of MB.

On the light of the overall improvement of MB removal capacity by TGSH at basic conditions, pH 9.0 was designated for conducting the other experiments.

3.3 Effect of contact time

The MB removal by TGSH was a time-controlled process (Fig. 3b). This behavior was assured by the rapid MB removal at retention time ranging from 5 to 30 min (7.3–8.3 mg/g, respectively) [40]. Such adsorption was related to the plentiful availability of unoccupied binding sites on the TGSH surface ready for interaction with MB ions [4], while the MB adsorption rate was decelerated ($q_t \approx 8.5$ mg/g) at $30 > t \leq 120$ min of equilibrium time owing to the decline in the accessible vacant sites on TGSH

Table 4 Textural parameters of TGSH obtained from the nitrogen adsorption isotherms

Sample	BET surface area (m^2/g)	Total pore volume (cm^3/g)	Average pore diameter (nm)
	S_{BET}	V_t	D_p
TGSH	5.41	0.0071	3.31

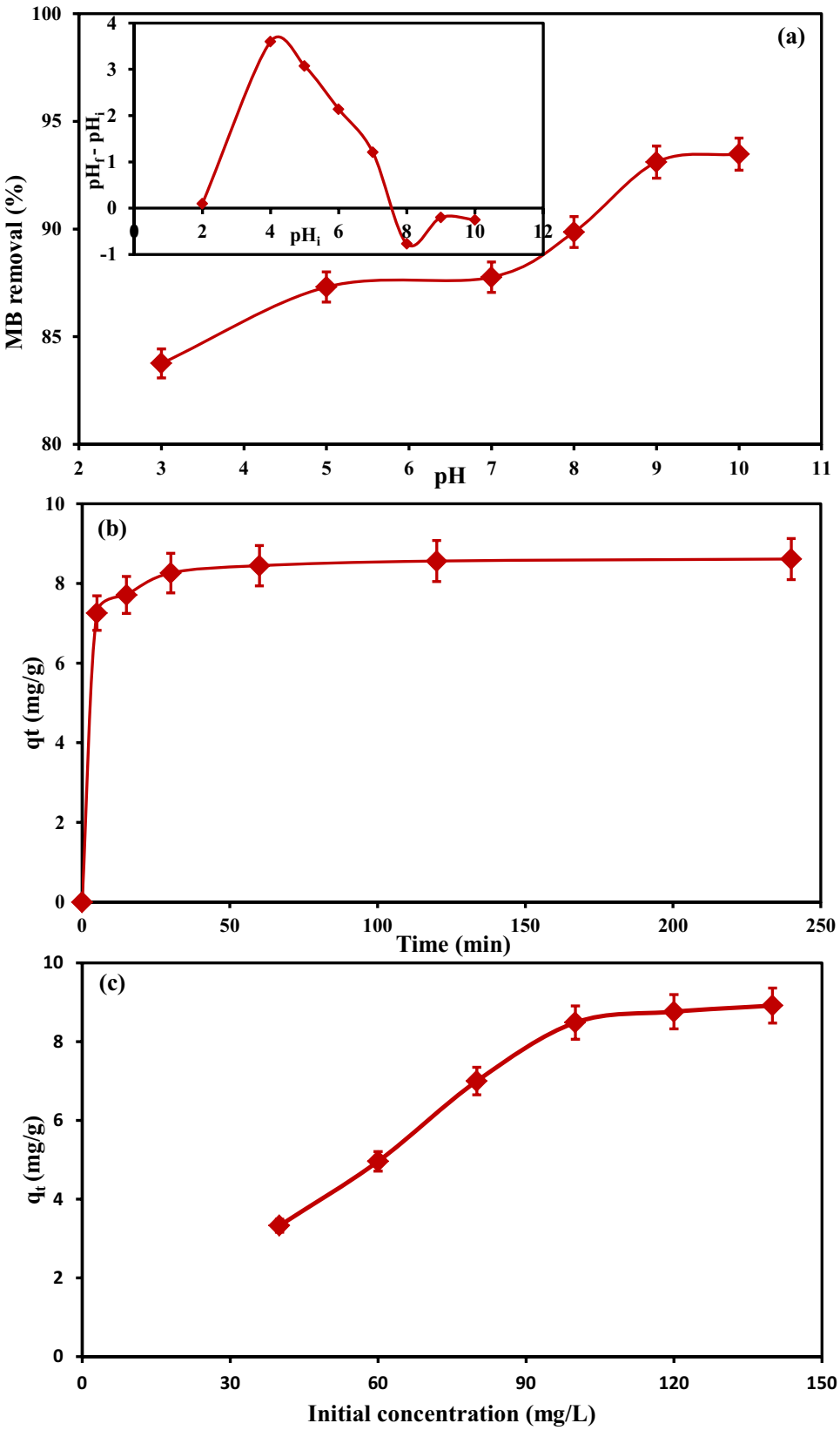

Fig. 3 Effect of pH on MB uptake by TGSH with its point of zero charge as inset (**a**). Effect of contact time on MB removal by TGSH (**b**), effect of initial concentration on MB removal by TGSH (**c**)

surface. Beyond 120 min of equilibrium time, insignificant increase in the removed amount of MB by the TGSH was recorded ($q_t \approx 8.6$ mg/g). Consequently, the rapid equilibrium nominates the TGSH as a promising adsorbent for MB uptake and implies the chemical nature of MB adsorption. So, 120 min was consigned as an equilibrium time of MB adsorption by the TGSH for the subsequent experimental parameters.

3.4 Effect of initial concentration

The increase in the sorbate initial concentration from 40 to 100 mg/L improved the MB adsorbed amount (q_e) from 3.3 to 8.49 mg/g, respectively, per unit mass of the addressed TGSH (Fig. 3c). This improvement could be ascribed to the progressive improvement in the intensity of MB ions collisions with the linking sites of the TGSH at high initial concentration [21]. These collisions acted as driving forces that promote the allocation of the MB ions to the surface of TGSH [66, 70], whereas, the increase in MB initial concentration from 100 to 140 mg/L revealed a slight increase in q_e (from 8.49 to 8.91 mg/L, respectively) as an indication of equilibrium status. This was correlated with the saturation of binding active sites on the surface of TGSH with the adsorbed MB ions [70].

3.5 Effect of talc-graphite schist mass

The MB removal (*R*%) by different masses of the addressed TGSH (0.15–0.4 g) was carefully monitored (Fig. 4a, Table 2). The increase in the TGSH mass from 0.15 to 0.35 g was accompanied by an increase in the MB removal capacity from 57.9 to 98.8%, respectively. However, the utilization of 0.4 g of the TGSH was sufficient to remove all the MB

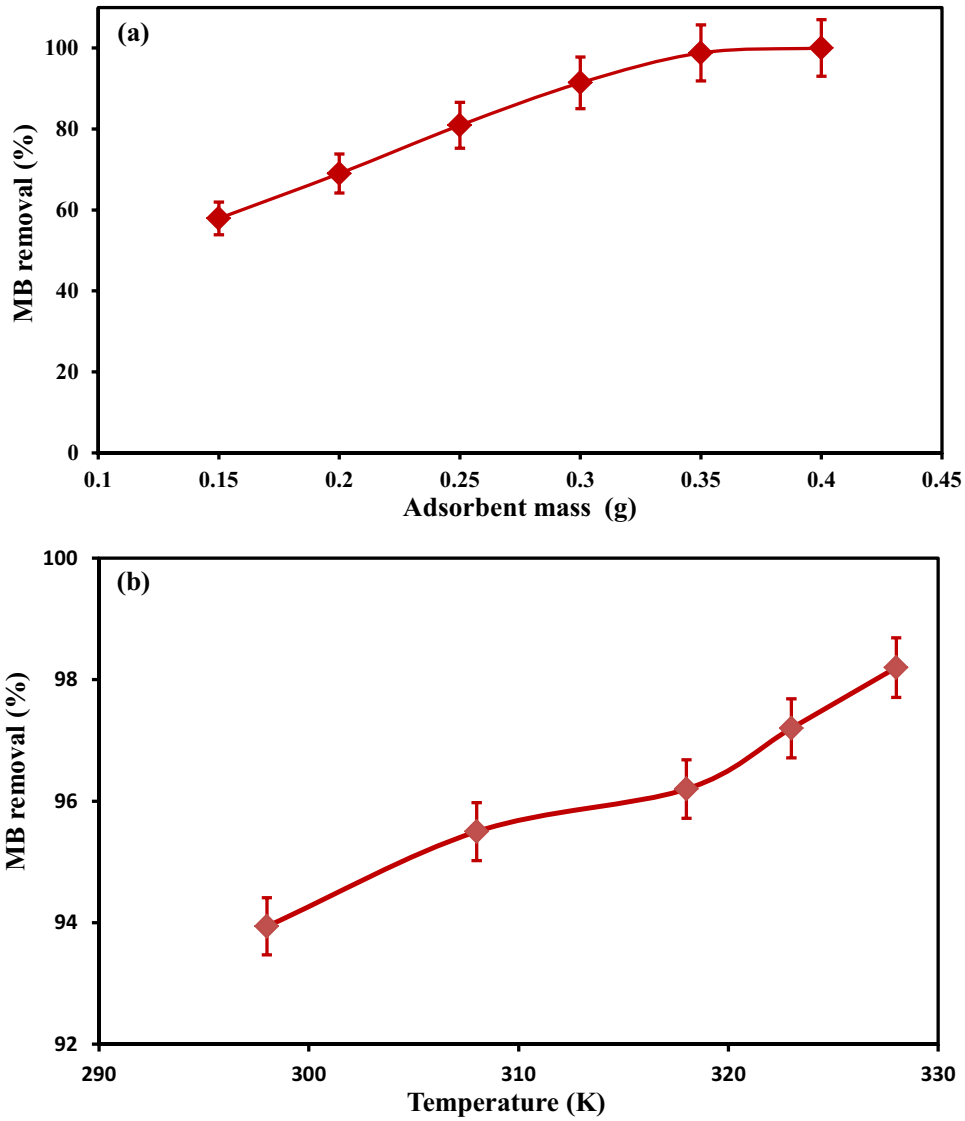

Fig. 4 Effect of absorbent mass on MB uptake by TGSH (**a**), effect of temperature on MB removal by TGSH (**b**)

ions from the solution (i.e., 100% removal capacity). This improvement in MB removal capacity till equilibrium with increasing the applied doses of the studied adsorbent was related to the approachability of plentiful unoccupied binding sites on the TGSH surface [59, 54].

3.6 Effect of temperature

The profile of MB removal by TGSH in a different range of temperatures (298–328 K) was carefully studied (Fig. 4b, Table 2). Raising the applied temperature from 298 to 328 K was accompanied by a progressive rise in MB removal capacity (*R*%) from 93.94 to 98.2%, respectively. This increase affirmed that the nature of MB adsorption by TGSH was endothermic [20, 52]. Moreover, the decrease in the solution viscosity with increasing the applied temperature probably improved the MB diffusion rate at the exterior boundary layer and hence within the TGSH pores [4].

3.7 Adsorption kinetics

The nonlinear forms of the "pseudo-1st-order, PFO" and "pseudo-2nd-order, PSO" equations were used to figure out the kinetics of MB adsorption by TGSH adsorbent (Table 5). The parameters of the nonlinear forms of the adopted models were determined by fitting the nonlinear curve of the plot of q_e versus C_e using Microsoft Excel Solver Tool. The estimated parameters of the applied equations are compiled in Table 6.

The MB adsorption process by the TGSH adsorbent was expressed well by PSO equation better than PFO (Fig. 5a), signifying that chemisorption is the potential rate-controlling step of MB adsorption process [35]. This was evident from higher determination coefficient derived from the nonlinear regression of the former ($R^2 = 0.939$) than the latter ($R^2 = 0.653$) [75, 53]. Also, unlike the PFO, the very close matching between the calculated q_e that was derived from nonlinear regression of the PSO ($q_e^{cal} = 8.59$ mg/g) and the experimental q_e^{exp} (8.56 mg/g), confirms that the latter equation describes the MB adsorption data well (Table 6).

3.8 Adsorption mechanism

Since the above-mentioned kinetic models (PFO and PSO) were not able to identify the diffusion nature of the MB ions from the solution into the surface of the TGSH, intra-particle diffusion model [77] was applied to fulfill this mission. This model is expressed by the following equation:

$$q_t = k_p t^{1/2} + C$$

Table 5 Adsorption kinetics models for MB removal by TGSH

Kinetic model	Nonlinear form	Parameters	References
Pseudo-first order	$q_t = q_e(1 - \exp^{(-K_1 t)})$	q_t (mg/g): removed amount of MB at time *t* q_e (mg/g): equilibrium adsorption uptake k_1 (g/mg min): rate constant of the first-order adsorption	Langergren and Svenska [43]
Pseudo-second-order	$q_t = \frac{k_2 t (q_e)^2}{1 + k_2 q_e t}$	q_t (mg/g): removed amount of MB at time *t* q_e (mg/g): equilibrium adsorption uptake k_2 (g/mg min): rate constant of the second-order adsorption	Blanchard et al. [10]

Table 6 The kinetic parameters of the MB adsorption by TGSH

Initial MB concentration (mg/L)	$q_e^{(exp.)}$ (mg/g)	Kinetic models parameters					
		Pseudo-first-order			Pseudo-second-order		
		K_1 (g/mg min)	$q_e^{(Calc.)}$ (mg/g)	R^2	K_2 (g/mg min)	$q_e^{(Calc.)}$ (mg/g)	R^2
100	8.56	0.404	8.33	0.653	0.127	8.59	0.939

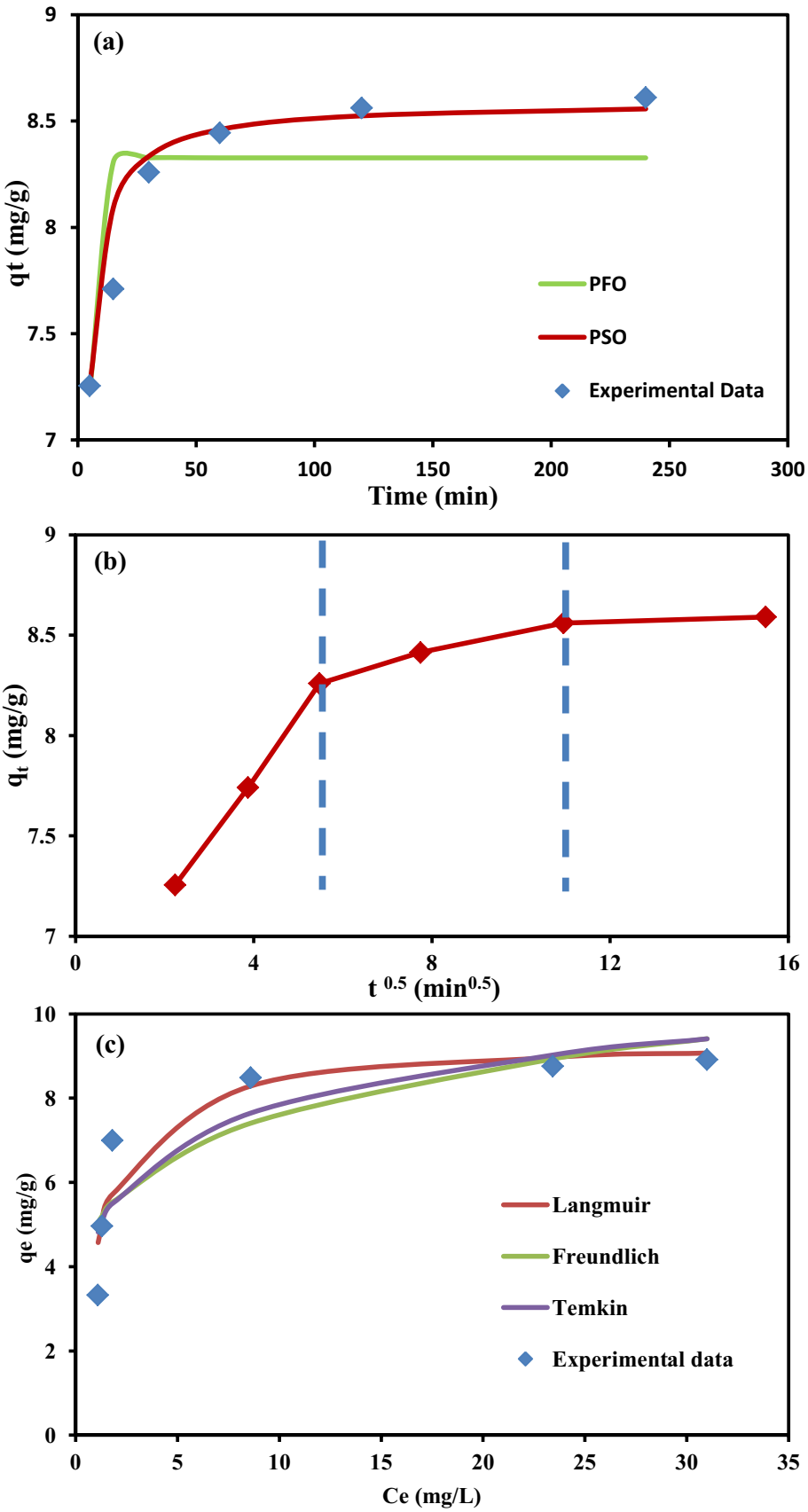

Fig. 5 Nonlinear plot of PFO and PSO kinetic models for MB adsorption by TGSH at 298 K (**a**), Intra-particle diffusion plot for MB removal by TGSH at 298 K (**b**), nonlinear plot of various isotherm models for MB adsorption by TGSH at 298 K (c)

where q_t (mg/g) is the removed amount of MB at time t, K_p (mg/g $min^{0.5}$) is the intra-particle diffusion rate constant, and C (mg/g) is intercept of the line which reflects the thickness of the boundary layer.

The intra-particle diffusion equation was graphically presented by plotting of q_t versus $t^{0.5}$ (Fig. 5b). The obtained multi-linear plot plus the 7.97 mg/g value of the C constant confirmed that MB removal by the TGSH was not mainly described by intra-particle diffusion, but various diffusion sorts may be involved [3, 28, 61, 80, 81]. The C constant value measures the degree of surface sorption participation in the rate-controlling step of MB adsorption [19, 51]. The steep–slope part (1st stage) of the multi-linear plot reflects the very rapid MB adsorption by the binding sites of TGSH, where boundary layer diffusion or exterior mass transfer effect could be the controller of MB adsorption [76, 55], whereas the gentle-slope part (2nd stage) implies gradual adsorption of MB by the addressed TGSH and assures that intra-particle diffusion was the principal mechanism in this stage [4]. So, the linear plot of the 2nd stage was used to determine the K_p (0.055 mg/g $min^{0.5}$) and C and R^2 (0.987) parameters of the intra-particle diffusion equation [17]. The plateau part of the multi-stage plot (3rd stage) reflects the state of equilibrium with approximately constant rate of MB adsorption by the TGSH.

3.9 Adsorption isotherms

The nonlinear forms of two-parameter modeling "Langmuir, Freundlich and Temkin" were applied in this work to elucidate the nature of interaction between the studied MB and the addressed TGSH (Table 7). The parameters of the nonlinear regression of these models were deduced by fitting the nonlinear curve of the plot C_e versus q_e using Microsoft Excel Solver tool (Fig. 5c, Table 8). The nonlinear modeling is more favorable because linearization results in diverse, estimation errors inherent bias and fit distortions [39].

Table 7 Adsorption isotherm models for MB removal by TGSH

Isotherm model	Nonlinear form	Parameters	References
Langmuir	$q_e = \frac{q_{max} b C_e}{1+bC_e}$	C_e (mg/L): equilibrium concentration of the resting MB in the solution q_e(mg/g): removed amount of MB at equilibrium q_{max} (mg/g): maximum adsorption capacity b (L/mg): Langmuir constant	Langmuir [44]
	$R_L = 1/(1 + bC_0)$ $R_L > 1$ (unfavorable adsorption) $R_L = 1$ (linear adsorption) $(0 < R_L < 1$ (favorable adsorption) $R_L = 0$ (irreversible adsorption	R_L: equilibrium parameter of Langmuir equation C_0: initial MB concentration	Weber and Chakravorti [78]
Freundlich	$q_e = K_F(C_e^{1/n})$	C_e (mg/L): equilibrium concentration of the resting MB in the solution q_e(mg/g): removed amount of MB at equilibrium K_F (mg/g): MB adsorption capacity n: heterogeneity factor	Freundlich [25]
Temkin	$q_e = B \ln A(C_e)$ $B = RT/b$	A (L/g): Temkin isotherm constant (the equilibrium binding constant corresponding to the maximum binding energy) B (J/mol): Temkin constant related to heat of sorption b: Temkin isotherm constant R: the gas constant (8.314 J/mol K) T: the absolute temperature at 298 K	Tempkin and Pyzhev [72]

Table 8 The isotherm parameters of the MB removal by TGSH

Initial MB concentration (mg/L)	Isotherm models parameters								
	Langmuir			Freundlich			Temkin		
	q_{max} (mg/g)	b (L/mg)	R^2	$1/n$	K_F (mg/g)	R_2	B (J/mol)	A (L/g)	R^2
40–140	9.41	0.859	0.876	0.187	4.96	0.752	1.37	30.36	0.793

On the light of the determination coefficient (R^2) data of the nonlinear regressions of the addressed models, Langmuir ($R^2 = 0.876$) explained the equilibrium data of MB ions adsorption by TGSH better than both Temkin ($R^2 = 0.793$) and Freundlich ($R^2 = 0.752$) models. This confirms the homogeneous nature (i.e., mono-layer adsorption) of MB adsorption by the isoenergetic active sites of the TGSH [17, 29, 36, 37]. The dimensionless separation factor (R_L) of Langmuir equation was estimated from the equation given in Table 7. The R_L values were ranging from 0.008 to 0.028 (favorable, $0 < R_L < 1$) designating the applicability of Langmuir to express the MB adsorption data well by TGSH. Moreover, the q_{max} value was 9.41 mg/g. Although the apparent low q_{max} was ascribed to the reduced surface area of the TGSH, the tempting low cost (100 EGP/t) of this adsorbent can compensate such MB removal efficiency. A comparison of the q_{max} of the investigated TGSH with those of the other adsorbents that were used for the remediation of MB in previous studies is compiled in Table 9. This comparison indicated that the raw TGSH is a promising low-cost MB adsorbent.

3.10 Characterization of the spent talc-graphite schist

SEM, EDS, FT-IR and XRD characterization of the spent TGSH was conducted to detect any morphological, chemical and/or structural changes occurred as a result of the interaction of the active site (functional groups) on the adsorbent surface with the ionized MB molecules.

SEM of the spent TGSH revealed the appearance of evenly distributed nanosize (150–200 nm) spherical particles on the adsorbent surface in monolayer style (Fig. 6a). The development of these particles on the surface of the TGSH indicated the MB homogenous adsorption by the addressed adsorbent as discussed above. EDS analysis of the spent TGSH affirmed the presence of *S* (0.05%) besides the main components of the studied adsorbent (Fig. 6b).

The FT-IR spectral pattern of the spent TGSH exhibited positive or negative shift in the frequency of its main functional groups with slight increase in the intensities of these groups (Fig. 7a). These changes confirmed the incorporation of the TGSH linking sites in the MB adsorption [6, 46].

The XRD of the spent TGSH encountered a slight shift in the majority of peaks position to high 2θ angle side (0.08°–0.13°), with noticeable increase in the intensity of some peaks as a result of MB adsorption (Fig. 7b). These structural disturbances can be ascribed to the incorporation of the MB ions into the internal structure of the TGSH [6]. Also the degree of amorphous noise that was related to the organic content of the TGSH was increased after uploading of the TGSH with MB molecules.

4 Conclusion

The following conclusions could be depicted:

- TGSH is a natural organo-mineral homogenous complex produced by long-term metamorphic processes

Table 9 Adsorption capacity for MB by some natural, modified and synthetic materials in comparison with the addressed TGSH of the present study: qmax obtained from the Langmuir constant

Adsorbent	Adsorption capacity q_{max} (mg/g)	Removal %	Initial Conc. (mg/L)	Dose (g)	Equilibrium time (m)	References
Co_3O_4/SiO_2 nanocomposite	53.87	95.7	20	0.04	30	Abdel Ghafar et al. [1]
Moroccan illitic clay	13.7	–	30	0.02	60	Amrhar et al [7]
Ephedra strobilacea char (ESC)	31.055	91.5	50	0.05	40	Agarwal et al [4]
Phosphoric acid modified *Ephedra strobilacea* char (ESP)	21.88	94.5	60	0.07	30	Agarwal et al. [4]
Zinc chloride modified *Ephedra strobilacea* char (ESZ)	37.174	93	60	0.05	60	Agarwal et al. [4]
Fe_3O_4/activated montmorillonite nanocomposite	106.38	99.47	120	0.5	25	Chang et al. [14]
Alginate/almond peanut biocomposite	22.8	90	30	0.1	120	Erfani and Javanbakht [23]
Sour lemon	52.4	92.8	5	2	120	Esmaeili and Foroutan [24]
Eucalyptus	53.5	93.4	5	2	120	
Sawdust of palm tree	54	95.8	5	2	120	
Bituminous coal	1.68	96.5	50	2	360	Huang et al. [31]
Iraqi red kaolin clay	240.4	99.8	100	0.1	150	Jawad and Abdulhameed [33]
TGSH	9.41	91.4	100	0.3	120	Present study

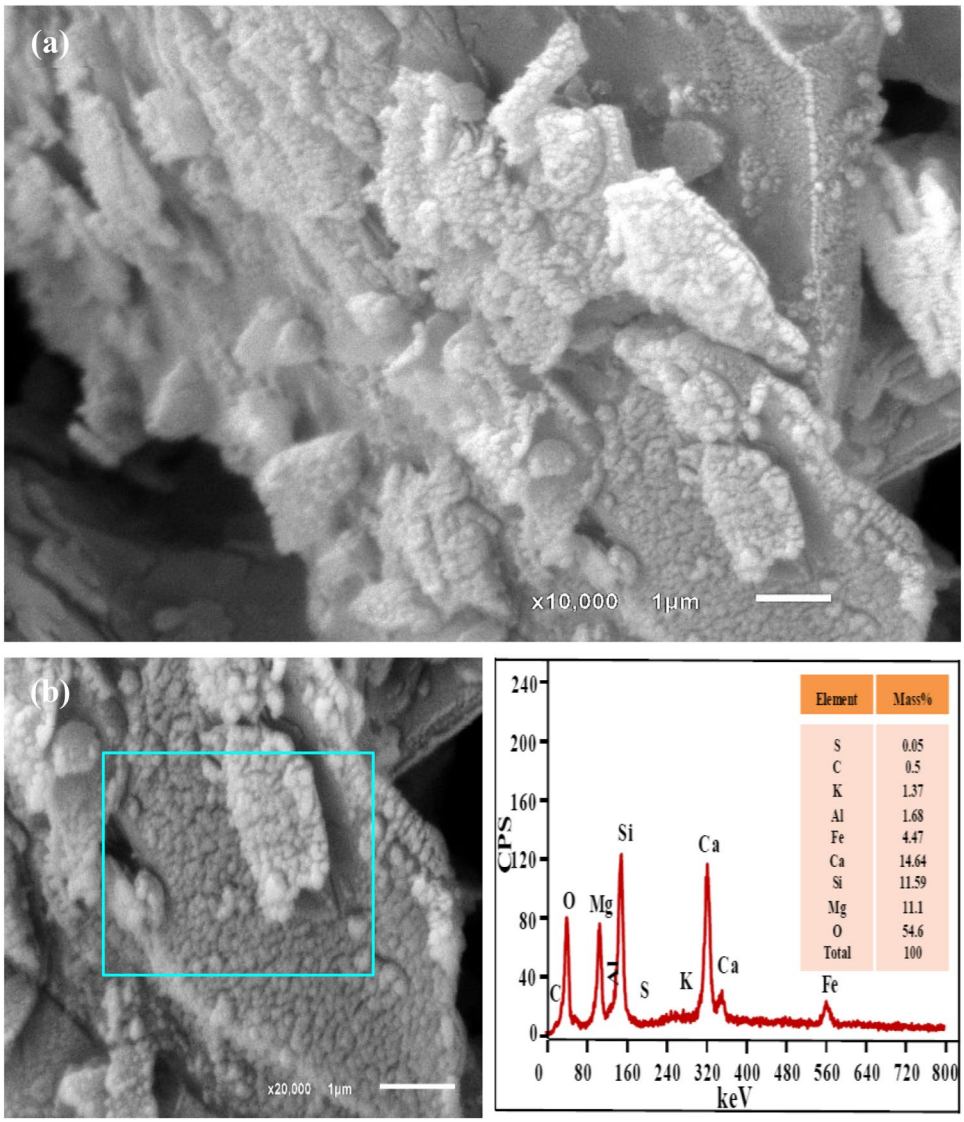

Fig. 6 SEM images for TGSH after MB removal (**a**), EDX of the TGSH after MB removal (**b**)

for the precursor organic matter-rich calcareous clays at the lowest T (573–632 K) and P (1–3 Kbars) of the green schist facies.

- TGSH is macroporous material with poor geometrical parameters ($S_{BET} \approx 5.41$ m^2/g, $V_t \approx 0.0071$). This could be attributed to the close packing of its mineral constituents during the experienced regional metamorphism (i.e., high temperature and directed pressure).
- As a result of the long-term metamorphic processes to which TGSH precursor was subjected, the dense packing of talc, organic matters and graphite particles resulted in their large van der Waals index and high surface hydrophobicity, invoking stronger hydrophobic influence in MB adsorption.
- The MB removal by TGSH was temperature-, time- and pH-controlled process of endothermic nature.
- The MB adsorption data were explained well by the PSO model ($R^2 = 0.939$) better than those of the PFO ($R^2 = 0.653$).
- Intra-particle diffusion with multi-linearity nature confirmed that the boundary layer/external mass transfer (At $0 < T \leq 30$ min) and intra-particle diffusions ($30 < T \leq 120$ min) were the main controlling steps in MB adsorption by TGSH.
- Langmuir model ($R^2 = 0.876$) explained the MB adsorption data better than the other investigated models. This may be attributed to the surface homogeneity that derived into monolayer adsorption of MB ions upon the TGSH surface.
- At $pH > pH_{PZC}$, the electrostatic interaction was the governing mechanism of MB adsorption by TGSH through the de-protonation of its oxygen- and nitrogen-bearing

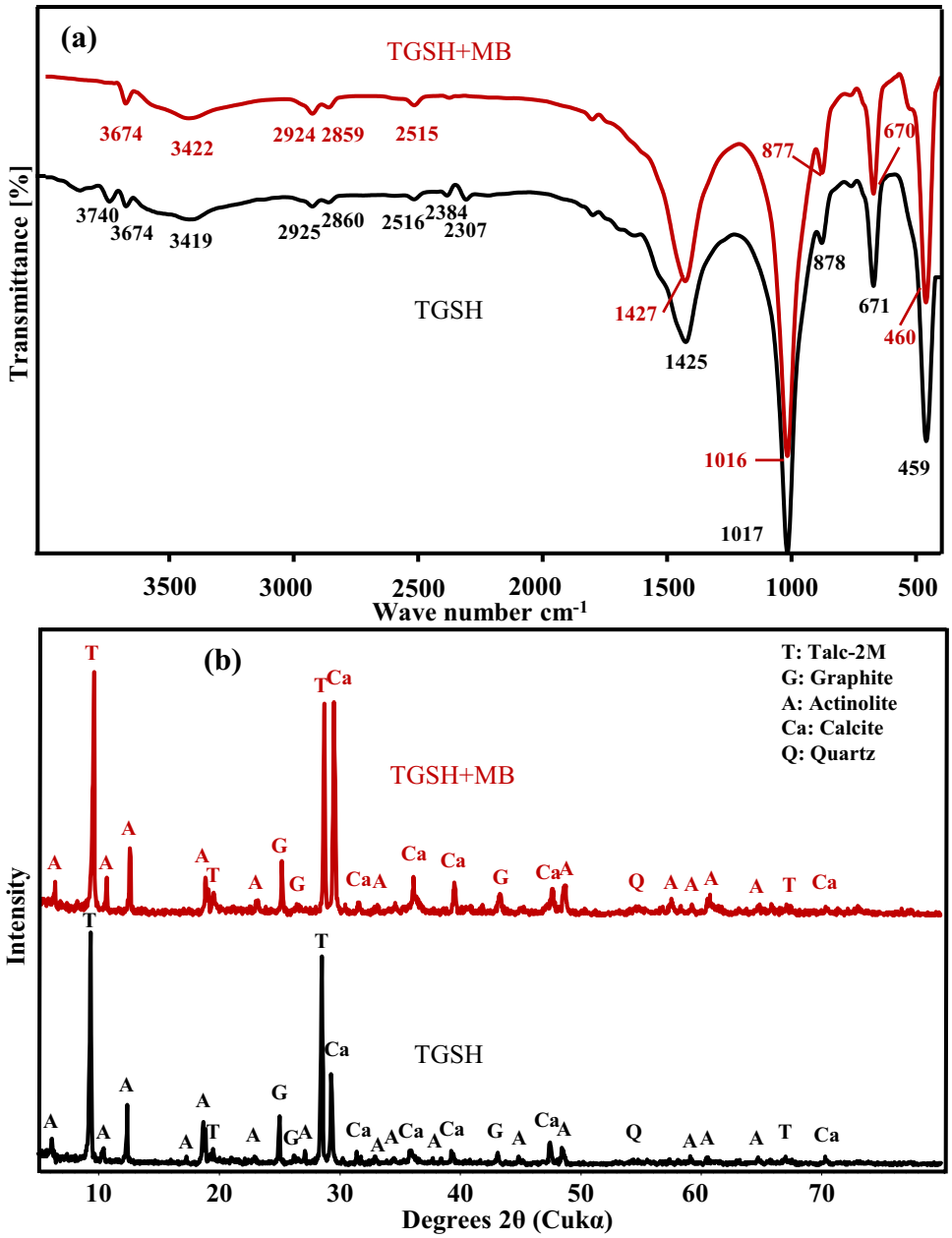

Fig. 7 FT-IR spectra of TGSH before and after MB removal (**a**), XRD pattern of TGSH before and after MB removal (**b**)

groups. Meanwhile, dipole–dipole and Yoshida hydrogen bonding interactions can account for the MB adsorption by TGSH, especially at pH < pH_{PZC}.

- Finally, TGSH is hazard-less natural adsorbent with huge availability in Egypt that approved acceptable workability for MB adsorption irrespective of the prevailing pH conditions (with some privilege in the basic medium over the acidic one) for a very tempting cost (100 EGP/t).

Acknowledgements The author of this work is appreciative for Mr/ Mostafa Abdel Azim for his effort in conducting the XRF analysis. Thanks also extended to Associate Prof./Rehab Khaleed for the fruitful discussion.

Compliance with ethical standards

Conflict of interest On behalf of all authors, the corresponding author states that there is no conflict of interest.

References

1. Abdel Ghafar HH, Ali GAM, Fouad OA, Makhlouf SA (2013) Enhancement of adsorption efficiency of methylene

blue on Co_3O_4/SiO_2 nanocomposite. Desalin Water Treat 53(11):2980–2989
2. Abdulhameed AS, Jawad AH, Mohammad A-T (2019) Synthesis of chitosan-ethylene glycol diglycidyl ether/TiO_2 nanoparticles for adsorption of reactive orange 16 dye using a response surface methodology approach. Bioresour Technol 293:122071
3. Abdulhameed AS, Mohammad A-T, Jawad AH (2019) Application of response surface methodology for enhanced synthesis of chitosan tripolyphosphate/TiO2 nanocomposite and adsorption of reactive orange 16 dye. J Clean Prod 232:43–56
4. Agarwal S, Tyagi I, Gupta VK, Ghasemi N, Shahivand M, Ghasemi M (2016) Kinetics, equilibrium studies and thermodynamics of methylene blue adsorption on *Ephedra strobilacea* saw dust and modified using phosphoric acid and zinc chloride. J Mol Liq 218:208–218
5. Akhair SHM, Harun Z, Basric H, Ahmad RAR, Rashid AQA, Azhar FH (2018) Hydrophobicity properties of graphite and reduced graphene oxide of the polysulfone (PSf) mixed matrix membrane. IJE Trans B Appl 31(8):1381–1388
6. Al-Ghouti MA, Al-Degs YS, Khraisheh MAM, Ahmad MN, Allen SJ (2009) Mechanisms and chemistry of dye adsorption on manganese oxides-modified diatomite. J Environ Manag 90:3520–3527
7. Amrhar O, Nassali H, Elyoubi MS (2015) Adsorption of a cationic dye, methylene blue, onto moroccan illitic clay. J Mater Environ Sci 6(11):3054
8. Barrett EP, Joyner LG, Halenda PP (1951) The determination of pore volume and area distributions in porous substances. I. Computations from nitrogen isotherms. J Am Chem Soc 73:373–380
9. Bishady AM (2017) Mineralogy of graphite from the graphite-bearing schists of Wadi Lawi, South Eastern Desert. Egypt JGRE 4:178–187
10. Blanchard G, Maunaye M, Martin G (1984) Removal of heavy metals from waters by means of natural zeolites. Water Res 18(12):1501–1507
11. Brauner S, Emmet PH, Teller E (1938) Adsorption of gases in multimolecular layers. J Am Chem Soc 60:309–319
12. Burgess-Clifford CE, Narayanan DL, Essendelft DTV, Jain P, Sakti A, Lueking AD (2009) The effect of calcination on reactive milling of anthracite as potential precursor for graphite production. Fuel Process Technol 90:1515–1523
13. Capar G, Yetis U, Yilmaz L (2006) Membrane based strategies for the pre-treatment of acid dye bath wastewaters. J Hazard Mater 135:423–430
14. Chang J, Ma J, Ma Q, Zhang D, Qiao N, Hu M, Ma H (2016) Adsorption of methylene blue onto Fe3O4/activated montmorillonite nanocomposite. Appl Clay Sci 119(1):132–140
15. Chang P, Jiang W, Li Z, Kuo C, Jean J, Chen W, Lv G (2014) Mechanism of amitriptyline adsorption on Ca-montmorillonite (SAz-2). J Hazard Mater 277:44–52
16. Cheah W, Hosseini S, Khan MA, Chuah TG, Choong TSY (2013) Acid modified carbon coated monolith for methyl orange adsorption. Chem Eng J 215–216:747–754
17. Chen S, Zhang J, Zhang C, Yue Q, Li Y, Li C (2010) Equilibrium and kinetic studies of methyl orange and methyl violet adsorption on activated carbon derived from Phragmites australis. Desalination 252:149–156
18. Chen ZX, Jin XY, Chen Z, Megharaj M, Naidu R (2011) Removal of methyl orange from aqueous solution using bentonite-supported nanoscale zero-valent iron. J Colloid Interface Sci 363:601–607
19. Deng H, Lu J, Li G, Zhang G, Wang X (2011) Adsorption of methylene blue on adsorbent materials produced from cotton stalk. J Chem Eng 172:326–334
20. Djilani C, Djazi RZF, Bouchekima B, Lallam A, Modarressi A, Rogalski M (2015) Adsorption of dyes on activated carbon prepared from apricot stones and commercial activated carbon. J Taiwan Inst Chem Eng 53:112–121
21. Dod R, Banerjee G, Saini DR (2015) Removal of methylene blue (MB) dye from water environment by processed Jowar Stalk [*Sorghum bicolor* (L.) Moench] adsorbent. Clean Technol Environ Policy 17:2349–2359
22. Dogan M, Alkan M, Türkyilmaz A, Özdemir Y (2004) Kinetics and mechanism of removal of methylene blue by adsorption onto perlite. J Hazard Mater B109:141–148
23. Erfani M, Javanbakht V (2018) Methylene blue removal from aqueous solution by a biocomposite synthesized from sodium alginate and wastes of oil extraction from almond peanut. Int J Biol Macromol 114:244–255
24. Esmaeili H, Foroutan R (2018) Adsorptive behavior of methylene blue onto sawdust of sour lemon, date palm, and eucalyptus as agricultural wastes. J Dispers Sci Technol 40(7):990–999
25. Freundlich HMF (1906) Over the adsorption in solution. J Phys Chem 57:385–471
26. Gong J-L, Wang B, Zeng G-M, Yang C-P, Niu C-G, Niu Q-Y, Zhou W-J, Liang Y (2009) Removal of cationic dyes from aqueous solution using magnetic multi-wall carbon nanotube nanocomposite as adsorbent. J Hazard Mater 164:1517–1522
27. Guibal E, Roussy J (2007) Coagulation and flocculation of dye-containing solutions using a biopolymer (Chitosan). React Funct Polym 67:33–42
28. Gusain D, Srivastava V, Sillanpää M, Sharma YC (2016) Kinetics and isotherm study on adsorption of chromium on nano crystalline iron oxide/hydroxide: linear and nonlinear analysis of isotherm and kinetic parameters. Res Chem Intermed 42:7133–7151
29. Hameed BH (2009) Spent tea leaves: a new non-conventional and low-cost adsorbent for removal of basic dye from aqueous solutions. J Hazard Mater 161:753–759
30. Hassan SM, El Kazzaz YA, Taha MM, Mohammad AT (2017) Late Neoproterozoic basement rocks of Meatiq area, Central Eastern Desert, Egypt: petrography and remote sensing characterizations. J Afr Earth Sci 131:14–31
31. Huang B, Zhao R, Xu H, Deng J, Li W, Wang J, Yang H, Zhang L (2019) Adsorption of methylene blue on bituminous coal: adsorption mechanism and molecular simulation. ACS Omega 4:14032–14039
32. Jawad AH, Abdul Mubarak NS, Abdulhameed AS (2020) Tunable Schiff's base-cross-linked chitosan composite for the removal of reactive red 120 dye: adsorption and mechanism study. Int J Biol Macromol 142:732–741
33. Jawad AH, Abdulhameed A (2020) Mesoporous Iraqi red kaolin clay as an efficient adsorbent for methylene blue dye: adsorption kinetic, isotherm and mechanism study. Surf Interfaces 18:100422
34. Jawad AH, Alkarkhi AFM, Abdul Mubarak NS (2014). Photocatalytic decolorization of methylene blue by an immobilized TiO_2 film under visible light irradiation: optimization using response surface methodology (RSM). Desalination Water Treat 1–12
35. Jawad AH, Ismail K, Ishak MAM, Wilson LD (2018) Conversion of Malaysian low-rank coal to mesoporous activated carbon: structure characterization and adsorption properties. Chin J Chem Eng 27(7):1716–1727
36. Jawad AH, Mamat NFH, Hameed BH, Ismail K (2019) Biofilm of cross-linked chitosan-ethylene glycol diglycidyl ether for removal of reactive red 120 and methyl orange: adsorption and mechanism studies. J Environ Chem Eng 7:102965
37. Jawad AH, Norrahma SSA, Hameed BH, Ismail K (2019) Chitosan-glyoxal film as a superior adsorbent for two structurally different reactive and acid dyes: adsorption and mechanism study. Int J Biol Macromol 135:569–581

38. Jawad AH, Abdul Mubarak NS, Ishak MAM, Ismail K, Nawawi WI (2016) Kinetics of photocatalytic decolourization of cationic dye using porous TiO2 film. J Taibah Univ Sci 10:352–362
39. Khan TA, Khan EA (2015) Removal of basic dyes from aqueous solution by adsorption onto binary iron-manganese oxide coated kaolinite: non-linear isotherm and kinetics modeling. Appl Clay Sci 107:70–77
40. Kim C, Zhang Z, Wang L, Sun T, Hu X (2016) Core–shell magnetic manganese dioxide nanocomposites modified with citric acid for enhanced adsorption of basic dyes. J Taiwan Inst Chem Eng 67:418–425
41. Kornaros M, Lyberatos G (2006) Biological treatment of wastewaters from a dye manufacturing company using a trickling filter. J Hazard Mater 136:95–102
42. Lafi R, Hafiane A (2016) Removal of methyl orange (MO) from aqueous solution using cationic surfactants modified coffee waste (MCWs). J Taiwan Inst Chem Eng 58:424–433
43. Langergren S, Svenska BK (1898) Veternskapsakad, Zur theorie der sogenannten adsorption geloester stoffe. Handlingar 24:1–39
44. Langmuir I (1918) The adsorption of gases on plane surfaces of glass, mica and platinum. J Am Chem Soc 40(9):1361–1403
45. Li H, An N, Liu G, Li J, Liu N, Jia M, Zhang W, Yuan X (2016) Adsorption behaviors of methyl orange dye on nitrogen-doped mesoporous carbon materials. J Colloid Interface Sci 466:343–351
46. Li Z, Chang P-H, Jiang W-T, Jean J-S, Hong H (2011) Mechanism of methylene blue removal from water by swelling clays. J Chem Eng 168:1193–1200
47. Liu H, Yuan P, Liu D, Bu H, Song H, Qin Z, He H (2018) Pyrolysis behaviors of organic matter (OM) with the same alkyl main chain but different functional groups in the presence of clay minerals. Appl Clay Sci 153:205–216
48. Ma J, Zhang J, Li D (2010) Removal of Methylene Blue by lava adsorption and catalysis oxidation. Environ Technol 31(3):267–276
49. Marcilla A, Gómez A, Menargues S (2005) TGA/FTIR study of the catalytic pyrolysis of ethylene-vinyl acetate copolymers in the presence of MCM-41. Polym Degrad Stab 89:145–152
50. Mastalerz M, He LL, Melnichenko YB (2012) Porosity of coal and shale: insights from gas adsorption and SANS/USANS techniques. Energy Fuel 26:5109–5120
51. Mittal H, Maity A, Ray SS (2015) Effective removal of cationic dyes from aqueous solution using gum ghatti-based biodegradable hydrogel. Int J Biol Macromol 79:8–20
52. Mohamed EA, Selim AQ, Zayed AM, Komarneni S, Mobarak M, Seliem MK (2019) Enhancing adsorption capacity of Egyptian diatomaceous earth by thermo-chemical purification: methylene blue uptake. J Colloid Interface Sci 534:408–419
53. Mohammad A-T, Abdulhameed AS, Jawad AH (2019) Box-Behnken design to optimize the synthesis of new cross-linked chitosan-glyoxal/TiO_2 nanocomposite: methyl orange adsorption and mechanism studies. Int J Biol Macromol 129:98–109
54. Mokhtari P, Ghaedi M, Dashtian K, Rahimi MR, Purkait MK (2016) Removal of methyl orange by copper sulfide nanoparticles loaded activated carbon: kinetic and isotherm investigation. J Mol Liq 219:299–305
55. Naiya TK, Bhattacharya AK, Mandal S, Das SK (2009) The sorption of lead (II) ions on rice husk ash. J Hazard Mater 163:1254–1264
56. Rida K, Bouraoui S, Hadnine S (2013) Adsorption of methylene blue from aqueous solution by kaolin and zeolite. Appl Clay Sci 83–84:99–105
57. Robati D, Mirza B, Ghazisaeidi R, Rajabi M, Moradi O, Tyagi I, Agarwal S, Gupta VK (2016) Adsorption behavior of methylene blue dye on nanocomposite multi-walled carbon nanotube functionalized thiol (MWCNT-SH) as new adsorbent. J Mol Liq 216:830–835
58. Saikia JB, Parasarathy G (2010) Fourier transform infrared spectroscopic characterization of kaolinite from Assam and Meghalaya, North Eastern India. J Mod Phys 1:2006–2010
59. Saleh TA, Al-Saadi AA, Gupta VK (2014) Carbonaceous adsorbent prepared from waste tires: experimental and computational evaluations of organic dye methyl orange. J Mol Liq 191:85–91
60. Seehra MS, Geddam UK, Schwegler-Berry D, Stefaniak AB (2015) Detection and quantification of 2H and 3R phases in commercial graphene-based materials. Carbon 95:818–823
61. Selim AQ, Mohamed EA, Mobarak M, Zayed AM, Seliem MK, Komarneni S (2018) Cr(VI) uptake by a composite of processed diatomite with MCM-41: Isotherm, kinetic and thermodynamic studies. Microporous Mesoporous Mater 260:84–92
62. Selim AQ, Mohamed EA, Seliem MK, Zayed AM (2018) Synthesis of sole cancrinite phase from raw muscovite: characterization and optimization. J Alloys Compd 762:653–667
63. Shan C, Zhang T, Liang X, Zhang Z, Wang M, Zhang K, Zhu H (2018) On the fundamental difference of adsorption-pores systems between vitrinite- and inertinite-rich anthracite derived from the southern Sichuan basin, China. J Nat Gas Sci Eng 53:32–44
64. Shao Y, Wang X, Kang Y, Shu Y, Sun Q, Li L (2014) Application of Mn/MCM-41 as an adsorbent to remove methyl blue from aqueous solution. J Colloid Interface Sci 429:25–33
65. Sharma P, Kaur R, Baskar C, Chung W-J (2010) Removal of methylene blue from aqueous waste using rice husk and rice husk ash. Desalination 259:249–257
66. Shiue A, Ma C-M, Ruan R-T, Chang C-T (2012) Adsorption kinetics and isotherms for the removal methyl orange from wastewaters using copper oxide catalyst prepared by the waste printed circuit boards. Sustain Environ Res 22(4):209–215
67. Singh D, Verma S, Gautam RK, Krishna V (2015) Copper adsorption onto synthesized nitrilotriacetic acid functionalized Fe_3O_4 nanoparticles: kinetic, equilibrium and thermodynamic studies. J Enviro Chem Eng 3:2161–2171
68. Sprynskyy M, Gadzała-Kopciuch R, Nowak K, Buszewski B (2012) Removal of zearalenone toxin from synthetics gastric and body fluids using talc and diatomite: a batch kinetic study. Colloids Surf B 94:7–14
69. Su Y, Jiao Y, Dou C, Han R (2014) Biosorption of methyl orange from aqueous solutions using cationic surfactant-modified wheat straw in batch mode. Desalin Water Treat 52:6145–6155
70. Subbaiah MV, Kim D-S (2016) Adsorption of methyl orange from aqueous solution by aminated pumpkin seed powder: kinetics, isotherms, and thermodynamic studies. Ecotoxicol Environ Saf 128:109–117
71. Tabak A, Afsin B, Caglar B, Koksal E (2007) Characterization and pillaring of a Turkish bentonite (Resadiye). J Colloid Interface Sci 313:5–11
72. Tempkin MJ, Pyzhev V (1940) Kinetics of ammonia synthesis on promoted iron catalysts. Acta Physicochim URSS 12:217–222
73. Thommes M, Kaneko K, Neimark AV, Olivier JP, Rodriguez-Reinoso F, Rouquerol J, Sing KSW (2015) Physisorption of gases, with special reference to the evaluation of surface area and pore size distribution (IUPAC Technical Report). Pure Appl Chem 87:9–10
74. Tran HN, You S-J, Chao H-P (2017) Insight into adsorption mechanism of cationic dye onto agricultural residues-derived hydrochars: negligible role of π-π interaction. Korean J Chem Eng 34(6):1708–1720
75. Wang L, Zhang J, Wang A (2011) Fast removal of methylene blue from aqueous solution by adsorption onto chitosan-g-poly (acrylic acid)/attapulgite composite. Desalination 266:33–39

76. Wang S, Zhu ZH (2006) Characterization and environmental application of an Australian natural zeolite for basic dye removal from aqueous solution. J Hazard Mater B136:946–952
77. Weber JC, Morris WJ (1962) Advances in water pollution research: removal of biologically resistant pollutant from waste water by adsorption. Proc Int Conf Water Pollut Symp Pergamon 2:231–266
78. Weber TW, Chakravorti RK (1974) Pore and solid diffusion models for fixed-bed adsorbers. AIChE J 20(2):228–238
79. Yee LF, Abdullah MP, Abdullah A, Ishak B, Abidin KNZ (2009) Hydrophobicity characteristics of natural organic matter and the formation of THM. MJAS 13(1):94–99
80. Zayed AM, Abdel Wahed MSM, Mohamed EA, Sillanpää M (2018) Insights on the role of organic matters of some Egyptian clays in methyl orange adsorption: isotherm and kinetic studies. Appl Clay Sci 166:49–60
81. Zayed AM, Selim AQ, Mohamed EA, Abdel Wahed MSM, Seliem MK, Sillanpää M (2017) Adsorption characteristics of Na-A zeolites synthesized from Egyptian kaolinite for manganese in aqueous solutions: response surface modeling and optimization. Appl Clay Sci 140:17–24
82. Zhang Y, Wang W, Zhang J, Liu P, Wang A (2015) A comparative study about adsorption of natural palygorskite for methylene blue. J Chem Eng 262:390–398
83. Zhao W, Wu Z, Wang D (2006) Ozone direct oxidation kinetics of cationic red X-GRL in aqueous solution. J Hazard Mater 137:1859–1865